ACS OMEGA

Open Access

http://pubs.acs.org/journal/acsodf

Article

Corn Silk Polysaccharide Reduces the Risk of Kidney Stone Formation by Reducing Oxidative Stress and Inhibiting COM Crystal Adhesion and Aggregation

Bao-Li Heng, Fan-Yu Wu,* Xin-Yi Tong, Guo-Jun Zou, and Jian-Ming Ouyang*

Cite This: *ACS Omega* 2024, 9, 19236−19249

Read Online

ACCESS | Metrics & More | Article Recommendations

ABSTRACT: The aim of this study is to explore the inhibition of nanocalcium oxalate monohydrate (nano-COM) crystal adhesion and aggregation on the HK-2 cell surface after the protection of corn silk polysaccharides (CSPs) and the effect of carboxyl group (−COOH) content and polysaccharide concentration. Method: HK-2 cells were damaged by 100 nm COM crystals to build an injury model. The cells were protected by CSPs with −COOH contents of 3.92% (CSP0) and 16.38% (CCSP3), respectively. The changes in the biochemical indexes of HK-2 cells and the difference in adhesion amount and aggregation degree of nano-COM on the cell surface before and after CSP protection were detected. Results: CSP0 and CCSP3 protection can obviously inhibit HK-2 cell damage caused by nano-COM crystals, restore cytoskeleton morphology, reduce intracellular ROS level, inhibit phosphoserine eversion, restore the polarity of the mitochondrial membrane potential, normalize the cell cycle process, and reduce the expression of adhesion molecules, OPN, Annexin A1, HSP90, HAS3, and CD44 on the cell surface. Finally, the adhesion and aggregation of nano-COM crystals on the cell surface were effectively inhibited. The carboxymethylated CSP3 exhibited a higher protective effect on cells than the original CSP0, and cell viability was further improved with the increase in polysaccharide concentration. Conclusions: CSPs can protect HK-2 cells from calcium oxalate crystal damage and effectively reduce the adhesion and aggregation of nano-COM crystals on the cell surface, which is conducive to inhibiting the formation of calcium oxalate kidney stones.

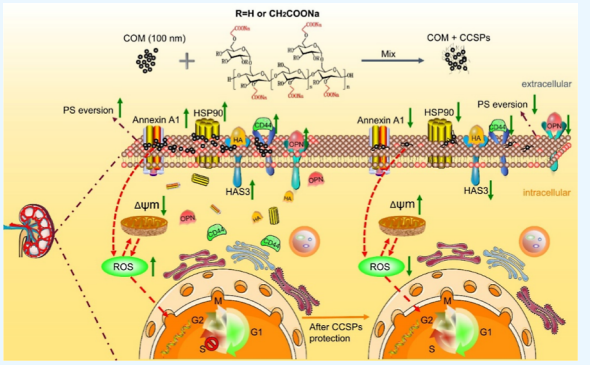

1. INTRODUCTION

Kidney stone is a common clinical disease, and its prevalence is increasing annually,[1] in which the incidence of calcium oxalate (CaOx) stones reaches 78%.[2] Our previous studies show that the cytotoxicity of nanocrystals is higher than that of micron crystals, while the cytotoxicity of calcium oxalate monohydrate (COM) crystals is significantly higher than that of calcium oxalate dihydrate crystals at the same concentration.[3]

The adhesion of COM crystals on the surface of renal tubular epithelial cells is one of the major causes of CaOx stone formation.[4] Damage to renal epithelial cells will promote the adhesion of COM crystals on the cell surface and increase the risk of kidney calculi formation. Studies have shown that hyaluronic acid (HA), osteopontin (OPN), and CD44 (cluster of differentiation 44) are highly expressed in damaged renal tubular epithelial cells.[5] These negatively charged adhesion molecules can adsorb Ca^{2+} in the solution and adhere to COM crystals with positive charges on the surface, thereby promoting crystal adhesion on the cell surface and leading to the occurrence of stones. In addition, the adhesion of COM crystals to injured renal tubular cells leads to the transformation of the cell cycle and slows down the process of DNA replication.[6] Therefore, reducing the damage and adhesion of COM crystals to renal epithelial cells is crucial to preventing the occurrence of kidney calculi.

Some inhibitors containing carboxyl (−COOH) can prevent cell adhesion to inorganic crystals. For example, citrate has been reported to have a unique adsorption mechanism for COM crystals, can effectively weaken COM adhesion, and can block the adhesion between crystals and renal epithelial cells.[7] Similarly, a simple heptapeptide sequence (peptide-7) designed by Liu et al.[8] can firmly adsorb hydroxyapatite and resist the washing action of phosphate buffer solution (PBS), and its strong binding ability may be attributed to a large number of negatively charged −COOH groups on peptide-7.

Received: January 4, 2024
Revised: February 24, 2024
Accepted: February 29, 2024
Published: April 17, 2024

Carboxymethylation is a common modification method to increase the −COOH content in polysaccharides. Carboxymethylated polysaccharides have properties superior to those of natural polysaccharides. For example, carboxymethylated fucoidan from *Laminaria japonica* has stronger antioxidant capacity in vitro than the noncarboxymethylated one.[9] Li et al.[10] found that the free-radical-scavenging activity of carboxymethylated derivatives has a high correlation with the increase in −COOH content. Sun et al.[11] showed that −COOH groups played a major role in the antitumor activity of *Ganoderma lucidum* polysaccharides.

Corn silk is the style and stigma of *Gramineae* corn. Polysaccharides extracted from corn silk have a wide range of biological activities, such as antioxidation,[12] antibacterial, hypolipidemic,[13] and hypoglycemic activities.[14] Our previous study[15] showed that corn silk polysaccharides (CSPs) can inhibit the crystal growth of CaOx and may be a potential drug for the prevention and treatment of kidney stones. Li et al.[16] increased the −COOH content of corn bran polysaccharide from 7.75% to 9.29−12.37%, and its antioxidant and antitumor activities were enhanced. However, no study on the changes of the antistone ability of carboxymethyl CSPs has been reported.

In this paper, the damage model of HK-2 cells was constructed by a nano-COM crystal, and the cells were protected by CSPs with carboxyl group contents of 3.92% (CSP0) and 16.38% (CCSP3), respectively. By detecting changes of the biochemical indexes of HK-2 cells before and after polysaccharide protection, the inhibitory effect of polysaccharide on oxidative damage of HK-2 cells induced by nano-COM was evaluated. By detecting the differences in the expression of adhesion molecules on the cell surface and observing the differences in the adhesion amount and aggregation degree of nano-COM on the cell surface, the mechanism and potential ability of polysaccharides to inhibit the formation of calcium oxalate kidney stones were studied, thereby providing a reference for the application of modified CSPs in the prevention and treatment of CaOx kidney calculi.

2. MATERIALS AND METHODS

2.1. Materials. *2.1.1. Reagents.* HK-2 cells (Shanghai Cell Bank of the Chinese Academy of Sciences); fetal bovine serum (FBS), DMEM/F-12 basal medium, PBS, penicillin and streptomycin (Pen Strep), and 0.25%-EDTA trypsin (Gibco); fluorescein isothiocyanate (FITC), 4,6-diamino-2-phenylindole (DAPI) staining solution, bovine serum albumin (BSA), 4% paraformaldehyde, reactive oxygen species (ROS) detection kit diluted 2′,7′-dichlorodihydro-fluorescein diacetate (DCFH-DA), mitochondrial membrane potential detection kit (JC-1), and Cell Counting Kit (CCK-8) (Beyotime Bio-Tech Co., Ltd.); osteopontin (OPN) antibody and sheep antimouse IgG-FITC (Boster Biological Technology Co., Ltd.); cytoskeleton green fluorescent probe (Keygen Bio-Tech Co., Ltd.); and Annexin V-FITC/PI apoptosis detection kit (Becton, Dickinson and Company) were used.

CSPs with carboxyl group content of 3.92% (CSP0) and 16.38% (CCSP3) were prepared according to the previous article.[17] All chemical reagents and solvents were purchased from the Guangzhou Chemical Reagent Factory (Guangzhou, China). Ultrapure water was used in all of the related experiments.

According to our previous reference,[18] COM crystals with a size of about 100 nm were synthesized, and the results of X-ray diffraction, Fourier transform infrared, and scanning electron microscopy (SEM) showed that they were all target crystals.

2.1.2. Apparatus. Confocal laser scanning microscopy (CLSM, 800Meta-DuoScan, Zeiss, Germany), inverted fluorescence microscope (Leica DMRA2, Germany), microplate reader (Gen5, Bio Tek, USA), flow cytometry (FACS Aria, BD, USA), SEM (JSM -TE300), optical microscope (OLYMPUS, CKX41, Japan), and Zetasizer Nano-ZS (Malvern, England) were used.

2.2. Experimental Methods. *2.2.1. Detection of Cell Viability, Nano-COM Particle Size, and Zeta Potential.*

1) Cell culture: HK-2 cells were cultured in DMEM-F12 medium containing 10% FBS in an incubator at 37 °C, 5% CO_2, and saturated humidity. The cells were passaged by trypsin digestion, incubated for 24 h, and reached 80% confluency before proceeding to the next step.

2) Detection of cell viability by CCK-8: the experimental models were divided into three groups: (1) normal control (NC): serum-free culture solution; (2) crystal damage group (COM): cells were damaged by adding 200 μg/mL nano-COM for 12 h; and (3) polysaccharide protection group: 10, 30, and 60 μg/mL polysaccharide CSP0 or CCSP3 were mixed with 200 μg/mL nano-COM for 15 min and then damaged cells for 12 h. Each experiment was set up with five multiple wells, which were detected by the CCK-8 method according to the determination method of the kit, and the OD value was measured at 450 nm. Cell viability (%) = A (treatment group)/A (control group) × 100.

3) Particle size and zeta potential detection of nano-COM before and after polysaccharide protection in culture solution: After mixing 10, 30, and 60 μg/mL CSP0 or CCSP3 with 200 μg/mL nano-COM in DMIM-F12 culture medium for 15 min, about 800 μL of suspension was injected into the sample pool. The zeta potential and hydrodynamic particle sizes were measured by a nanoparticle size and zeta potential analyzer. Parallel detection was carried out three times, and the average was taken.

2.2.2. Detection of the Intracellular ROS Level. The experimental models were divided into three groups: (1) NC: serum-free culture solution; (2) damage control (DC): cells were damaged by adding 200 μg/mL nano-COM for 12 h; and (3) polysaccharide protection group: 10, 30, and 60 μg/mL polysaccharide CSP0 or CCSP3 were mixed with 200 μg/mL nano-COM for 15 min and then damaged cells for 12 h.

DCFH-DA was added to the cells, incubated at 37 °C for 30 min, and then observed under a fluorescence microscope. The semiquantitative analysis of ROS fluorescence intensity was carried out using ImageJ software.

2.2.3. Observation of the Cytoskeleton. The experimental group was the same as that in 2.2.2. After the culture time was reached, the cells were fixed with 4% paraformaldehyde solution for 20 min. Actin-Tracker Green staining solution diluted with PBS containing 1−5% BSA and 0.1% Triton X-100 at a ratio of 1:100 was used to incubate the cells at room temperature for 20−60 min in the dark and then observed under a confocal microscope.

2.2.4. Detection of Phosphatidylserine Eversion. The experimental group was the same as 2.2.2; 100 μL of binding buffer and 10 μL of Annexin V-FITC (20 μg/mL) were added and kept away from light for 30 min at room temperature; a tube

https://doi.org/10.1021/acsomega.4c00110
ACS Omega 2024, 9, 19236−19249

without Annexin V-FITC was used as the negative control and quantitatively detected by flow cytometry.

2.2.5. Detection of the Cell Cycle. The experimental group was the same as 2.2.2, the cells were collected and resuspended in 300 μL of PBS, and 700 μL of precooled absolute ethanol was slowly added while shaking and fixed overnight at 4 °C in the dark. After centrifugation, the cells were resuspended in 500 μL of PBS for washing and then stained with 300 μL of PI in an incubator at 37 °C for 15 min, filtered, and detected by the computer.

2.2.6. Observation of Mitochondrial Membrane Potential Changes. The experimental group was the same as 2.2.2. After the incubation time was reached, JC-1 staining solution with a concentration of 20 μM was added, and the mixture was incubated for 30 min in the dark, washed twice with PBS, and observed by a laser confocal microscope.

2.2.7. Observation of OPN Expression. The experimental group was the same as 2.2.2. After the incubation time was reached, 4% paraformaldehyde was added to the fixed cells for 10 min, sheep serum was added to block them for 20 min, and then osteopontin antibody (1:100) was used to incubate at 4 °C overnight. After FITC-IgG (1:100) was added and the mixture incubated in the dark for 0.5 h, the nucleus was stained with DAPI for 10 min. Finally, the fluorescence was observed by a laser confocal microscope; the nucleus was blue and the OPN was green.

2.2.8. Western Blot. The cells were washed with PBS three times, and then RIPA was added to lyse the cells. Cells and reagents were collected with a cell scraper; the cells were fully dissolved by ultrasound and centrifuged at 4 °C 12,000 rpm for 15 min; the supernatant was transferred to a new 1.5 mL centrifuge tube, namely, the total protein solution. Total protein was loaded on 12% Tris-glycine SDS-polyacrylamide gel, which was run at 120 V for 1.5 h, and then transferred to a polyvinylidene fluoride (PVDF) membrane. It was sealed with 5% skim milk for 1 h, incubated with anti-Annexin A1, anti-CD44, anti-HAS3, and anti-HSP90 at 4 °C overnight, respectively, and with secondary antibody (1:10,000) at room temperature for 1.5 h, and finally developed.

2.2.9. Fluorescence Labeling of Calcium Oxalate Crystal. Preparation of FITC−COM fluorescent labeled crystals:[19] At 74 °C, 5 mL of 3-aminopropyl triethoxysilane was reacted with 0.05 g of COM in 50 mL of absolute ethyl alcohol for 3 h. Then, 25 mg of FITC was added to react for 6 h. Finally, it was washed with absolute ethyl alcohol and deionized water until it was free of FITC. The labeled nanoparticles (FITC−COM) were dried, and proper numbers of crystals were selected and detected by flow cytometry.

2.2.10. Observation of Crystal Adhesion on the Cell Surface. The experimental group was the same as 2.2.2. The cells were cultured at 4 °C for 6 h, stained with 300 μL of DiI for 10 min, stained with DAPI for 10 min, and fixed with 4% paraformaldehyde for 10 min. The distribution of nano-COM crystals on the cell membrane was observed by a laser confocal microscope.

2.2.11. Observation of Crystal Adhesion by SEM. The experimental group was the same as 2.2.2. Referring to our previous method,[20] the crystal adhesion on the cell surface was observed by a scanning electron microscope.

2.2.12. Quantitative Detection of Cells with Adhered Crystals. The experimental group was the same as 2.2.2. The cells were washed with cold PBS twice to remove the nonadhered and loosely adhered crystals. Cells with FITC signal can be regarded as cells with adhered crystals, and the percentage of FITC positive cells was determined by flow cytometry.

2.2.13. Statistical Analysis. Experimental data are expressed by at least three independent experiments and are displayed in the form of mean ± standard deviation ($\bar{x} \pm$ SD). Statistical analysis of the experimental results was performed using SPSS 13.0 software (SPSS Inc., Chicago, IL, USA), and one-way ANOVA was used to analyze the difference between the mean values of each experimental group and COM group. $P < 0.05$ indicates a significant difference. $P < 0.01$ indicated that the difference was very significant.

3. RESULTS

3.1. Decrease in Cell Viability Was Inhibited by CCSPs.

Figure 1 shows that CSPs with −COOH content of 3.92% (CSP0) and 16.38% (CCSP3) inhibited the change in HK-2 cell vitality caused by the nano-COM crystals. NC. Nano-COM concentration: 200 μg/mL. Protection time: 12 h. Compared with the COM group, $^{**}p < 0.01$.

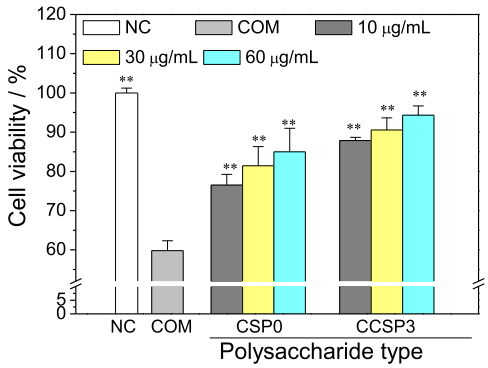

Figure 1. CSPs with −COOH contents of 3.92% (CSP0) and 16.38% (CCSP3) inhibited the change in HK-2 cell vitality caused by the nano-COM crystals. NC. Nano-COM concentration: 200 μg/mL. Protection time: 12 h. Compared with the COM group, $^{**}p < 0.01$.

Table 1. Particle Size (d) and Zeta Potential (ξ) after Mixing Nano-COM with Different Concentrations of CSP0 and CCSP3 in Culture Medium for 15 min (Average Result of Three Tests)

polysaccharide concentration/μg/mL	0	10	30	60
	CSP0			
d/nm	1065	1233	1344	1410
ξ/mV	−3.18	−7.64	−9.68	−12.6
	CCSP3			
d/nm	1065	1289	1398	1468
ξ/mV	−3.18	−11.6	−13.7	−16.2

(CSP0) and 16.38% (CCSP3) inhibit the change of HK-2 cell vitality caused by the nano-COM crystal. Compared with the NC group (100.00%), the cell viability (59.81%) after 12 h damaged by nano-COM decreased significantly ($p < 0.01$). The cell viability was improved (76.53∼94.31%) after CSP0 and CCSP3 protection at concentrations of 10, 30, and 60 μg/mL, respectively. The ability of CSP0 and CCSP3 to protect HK-2 cells from damage by nano-COM crystals was positively correlated with the concentration of polysaccharide and the −COOH content in CCSPs. For example, CCSP3 with the highest carboxyl content increased cell viability to 94.31% at 60 μg/mL.

To uncover the mechanism of this phenomenon, we have detected the particle size and zeta potential of nano-COM after

https://doi.org/10.1021/acsomega.4c00110
ACS Omega 2024, 9, 19236−19249

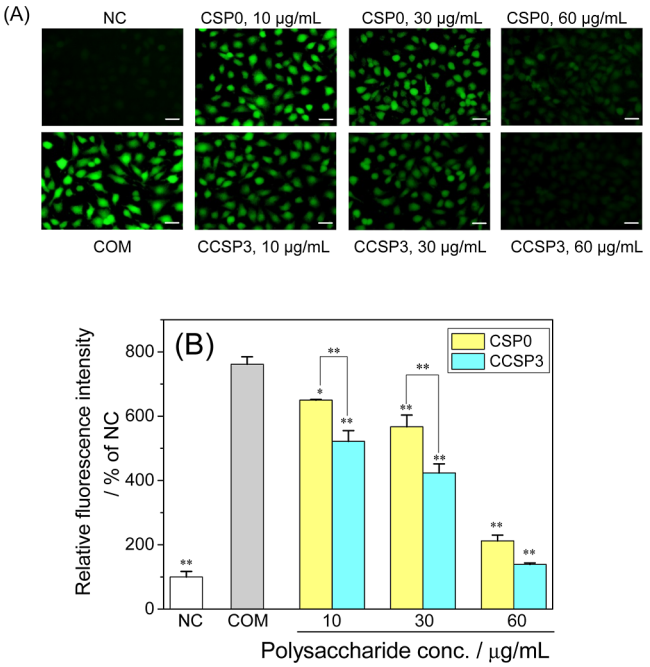

Figure 2. CSPs with different concentrations before and after carboxymethylation inhibited the change in ROS level caused by the nano-COM crystals. (A) ROS fluorescence photos (scale bars: 50 μm). (B) Relative fluorescence intensity histogram. NC. Nano-COM concentration: 200 μg/mL. Protection time: 12 h. Compared with the COM group, *$p < 0.05$; **$p < 0.01$.

mixing with different concentrations of CSP0 and CCSP3 for 15 min in culture medium (Table 1). The result shows that the nano-COM with a size of 100 nm increased significantly to 1065 nm in culture solution, and it further increased to 1233−1468 nm after interaction with polysaccharides. The zeta potential of nano-COM was −3.18 mV, but it became more negative (−7.64 to −16.2 mV) after interaction with polysaccharides. With the concentration increase of adsorbed polysaccharides or the increase of −COOH content in polysaccharides, the particle size of nano-COM increased, and the zeta potential became more negative.

3.2. Increase in Intracellular ROS Levels Was Inhibited by CCSPs. The ROS levels in the cells before and after CSP0 protection before carboxymethylation and CCSP3 with the highest −COOH content were detected by fluorescence microscopy, and the fluorescence intensity of ROS was semiquantitatively analyzed by ImageJ software. Figure 2 shows that almost no ROS green fluorescence was observed in normal cells, but the fluorescence of cells damaged by nano-COM crystals increased significantly ($p < 0.01$).

Under the protection of CSP0 and CCSP3, the degree of damage of nano-COM to cells was reduced and there was a concentration effect (Figure 2B). At the same concentration, CCSP3 can inhibit the increase of the ROS level induced by nano-COM crystals more than CSP0.

3.3. Cytoskeleton Destruction Was Inhibited by CCSPs. The cytoskeleton changes before and after CSP0 and CCSP3 protection were observed by CLSM (Figure 3). Normal HK-2 cells have a complete cytoskeleton and obvious actin microfilaments. After damage was induced by COM crystals, the cytoskeleton was deformed, the distribution of actin filaments was disordered, and the cells shrank.

With increasing concentrations, the cells protected by CSP0 or CCSP3 gradually had a fuller appearance and clear actin filaments. At the same concentration, the cytoskeleton protected by carboxymethylated polysaccharide (CCSP3) was more intact than that of CSP0.

3.4. Phosphatidylserine Eversion Was Inhibited by CCSPs. The effect of COM crystals on phosphoserine (PS) eversion on the HK-2 cell membrane before and after CSP0 and CCSP3 protection was detected by flow cytometry (Figure 4). The results showed that the PS eversion in the normal group was less (5.81%), while that in the COM crystal-damaged group was significantly increased (44.0%; $p < 0.01$). Under the protection of different concentrations of CSP0 or CCSP3, the PS eversion of cells was inhibited and there was a concentration effect (Figure 4B). Compared with CSP0, CCSP3 after carboxymethylation had a better effect on inhibiting PS eversion.

3.5. CCSPs Inhibit Cell Cycle Retention Caused by Nano-COM Crystals and Promote Cell DNA Synthesis. Figure 5 shows the changes in the HK-2 cell cycle before and after protection with different concentrations of CSP0 and CCSP3 by flow cytometry. Nano-COM crystals led to the decrease in the *G*1-phase cells and the increase in *S*-phase cells, that is, the damage induced by nano-COM crystals caused more cells to remain in the *S* phase and led to the decrease in *G*1-phase cells. The protective effects of polysaccharides reduced cell cycle retention and promoted the cycle transition from G2/M and S to G1; that is, polysaccharides accelerated the DNA synthesis process of HK-2 cells and promoted cell proliferation.

Compared with the CSP0 group, the CCSP3 protection group was more effective in maintaining cell cycle progression.

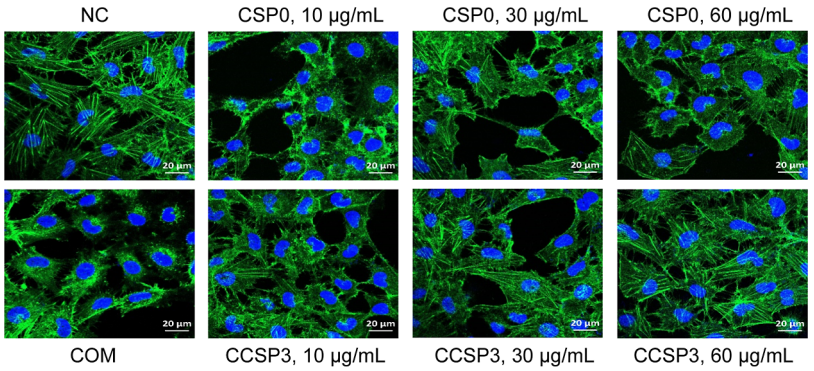

Figure 3. Cytoskeleton changes before and after CSP0 and CCSP3 protection were observed by CLSM. (Scale bars: 20 μm). NC. Nano-COM concentration: 200 μg/mL. Protection time: 12 h.

https://doi.org/10.1021/acsomega.4c00110
ACS Omega 2024, 9, 19236−19249

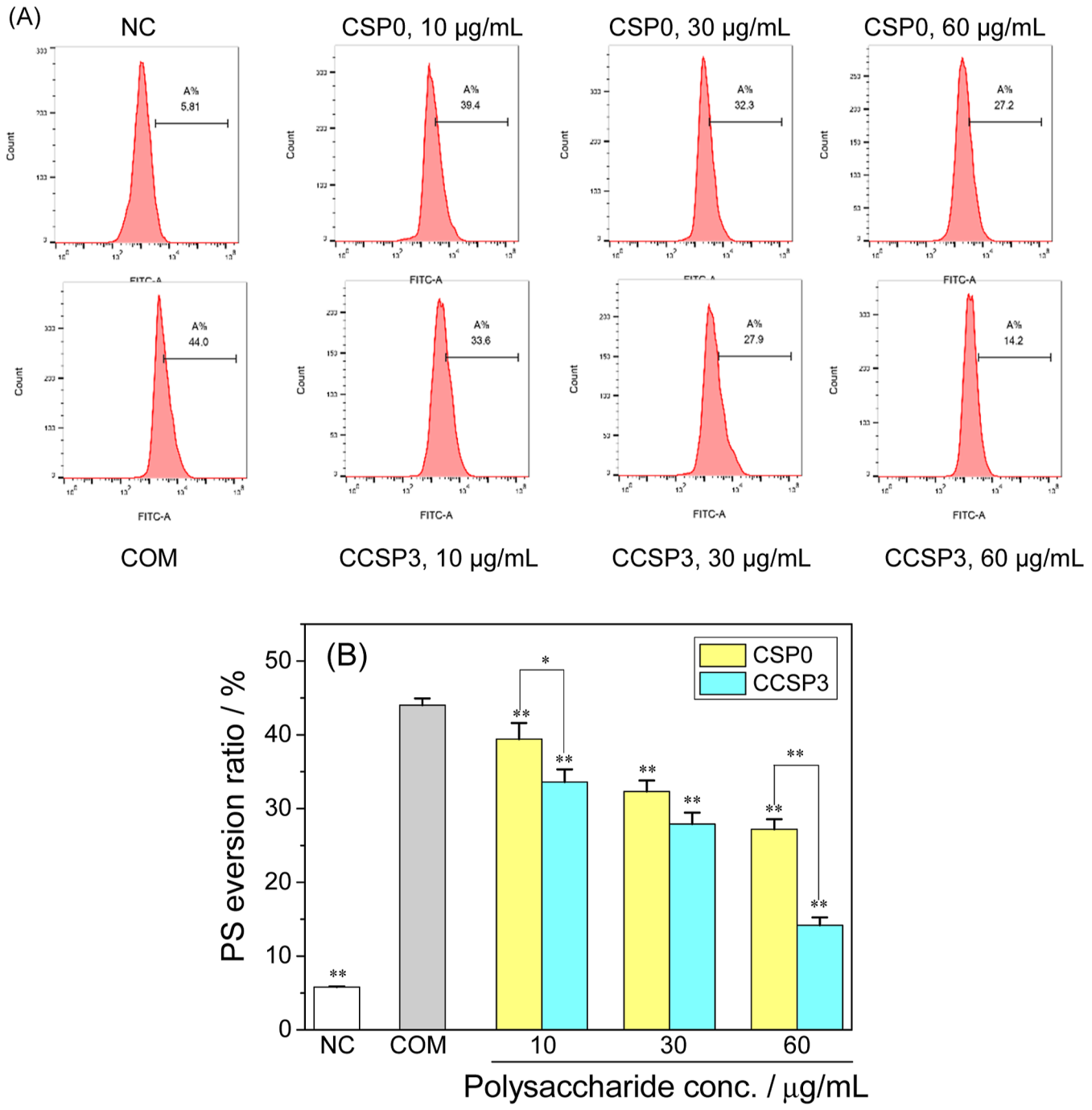

Figure 4. Effect of COM crystals on PS eversion on the HK-2 cell membrane before and after CSP0 and CCSP3 protection was detected by flow cytometry. (A) Flow cytometry histogram. (B) Quantitative histogram of PS eversion. NC. Nano-COM concentration: 200 μg/mL. Protection time: 12 h. Compared with the COM group, $^{*}p < 0.05$; $^{**}p < 0.01$.

For example, under the protection of 60 μg/mL CCSP3, the proportion of *G*1-phase cells increased from 53.4 to 74.7%, that of *S*-phase cells decreased from 30.8 to 17.6%, and that of *G*2/*M*-phase cells decreased from 15.8 to 7.72%. As such, the proportion of cells at the end of DNA synthesis and mitosis decreased, indicating that CCSP3 increased the proliferation rate of HK-2 cells.

3.6. Decrease in the Mitochondrial Membrane Potential Was Inhibited by CCSPs. The cationic lipophilic dye JC-1 was adopted as the fluorescence probe, and changes in red-green fluorescence were observed by laser confocal microscopy. The changes in the mitochondrial membrane potential of HK-2 cells before and after CSP0 and CCSP3 protection were detected. As shown in Figure 6, almost no green fluorescence was detected in normal cells. This result suggested that the mitochondrial membrane potential was high, and JC-1 was located in the mitochondrial matrix, forming polymers that emitted red fluorescence. Cells damaged by nano-COM have a strong green fluorescence and show only weak red fluorescence, indicating a low membrane potential and mostly monomeric JC-1.

Under the protection of CSP0 and CCSP3, the green fluorescence of cells became weaker, while the red fluorescence became stronger as the polysaccharide concentration increased.

https://doi.org/10.1021/acsomega.4c00110
ACS Omega 2024, 9, 19236−19249

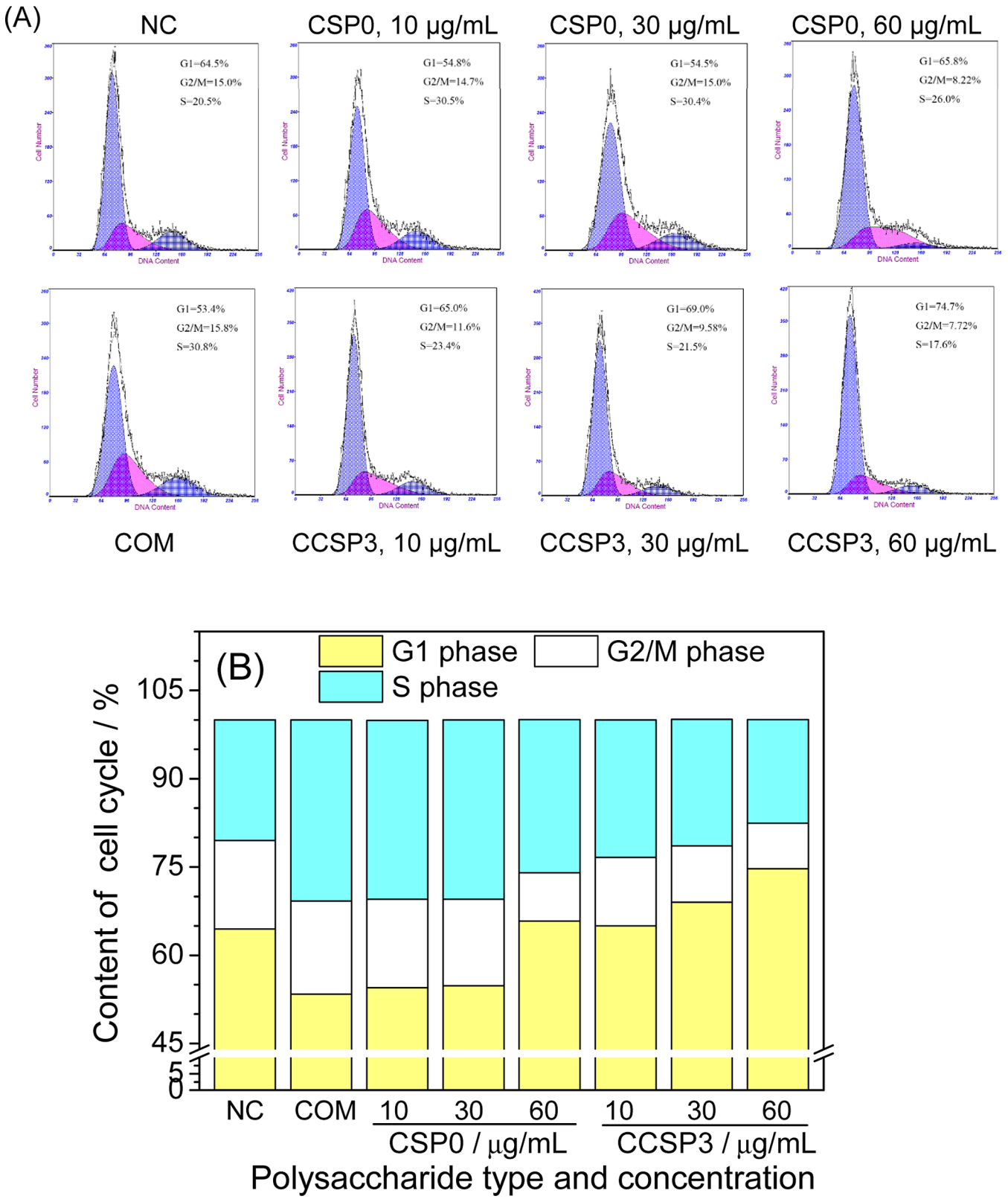

Figure 5. Changes in the HK-2 cell cycle before and after protection with different concentrations of CSP0 and CCSP3 by flow cytometry. (A) Cell cycle diagram. (B) Histogram of G1, S, and *G2/M* phase contents. NC. Nano-COM concentration: 200 μg/mL. Protection time: 12 h.

This result indicated that polysaccharides inhibited the decrease in the mitochondrial membrane potential caused by COM crystals and that the activity of CCSP3 was stronger than that of CSP0 (Figure 6B).

3.7. OPN Expression Was Decreased by CCSPs. OPN overexpression in the cell surface can increase the risk of CaOx stone formation by increasing its adhesion to COM crystals.[20] OPN expression was detected by immunofluorescence staining and semiquantitative image analysis (Figure 7). OPN green

https://doi.org/10.1021/acsomega.4c00110
ACS Omega 2024, 9, 19236−19249

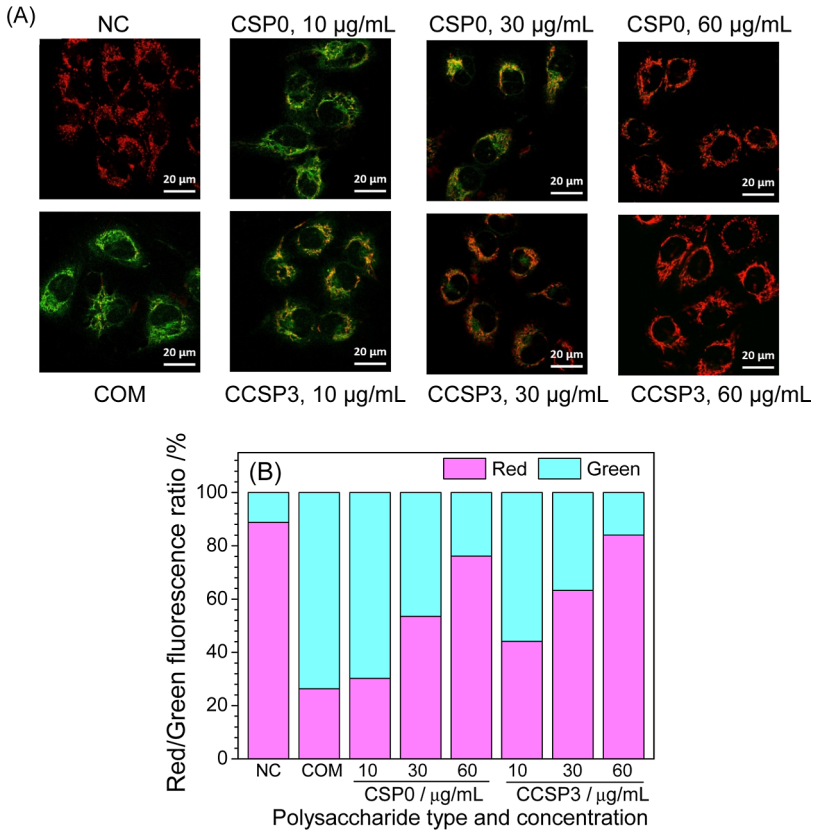

Figure 6. Changes in the mitochondrial membrane potential of HK-2 cells before and after CSP0 and CCSP3 protection were detected. (A) Red/green fluorescence confocal microscope pictures (scale bars: 20 μm). (B) Quantitative histogram of red/green fluorescence ratio. NC. Nano-COM concentration: 200 μg/mL. Protection time: 12 h.

fluorescence was detected in normal cells, while the green fluorescence of COM-damaged cells increased significantly ($p < 0.01$). The expression of OPN induced by nano-COM crystals can be inhibited by the protective effects of CSP0 or CCSP3, and there was a concentration effect (Figure 7B). At the same concentration, the protective effect of CCSP3 with a high −COOH content was better than that of CSP0.

3.8. Detection of the Expression of Adhesion-Related Proteins (Annexin A1, HSP90, HAS3, and CD44). Annexin A1, HA synthase 3 (HAS3), heat shock protein 90 (HSP90), and CD44 are adhesion-related proteins. Western blot analysis was used to detect the expression of these four proteins in HK-2 cells before and after polysaccharide protection (Figure 8). The results showed that the expression levels of the four proteins were significantly ($p < 0.01$) increased after being damaged by nano-COM. The expression of these proteins can be effectively inhibited after polysaccharide protection. For CD44, Annexin A1, and HAS, CCSP3 showed a better protection effect than CSP0. HSP90 expression in cells protected by CCSP3 and CSP0 had no difference ($p > 0.05$), but compared with COM-damaged cells, HSP90 expression in the two polysaccharide-protected cells was significantly different ($p < 0.05$).

The above results indicated that CSP0 and CCSP3 could inhibit the increase in the level of adhesion-related protein expression induced by COM crystals.

3.9. Observation of Crystal Distribution on the Cell Surface. Nanoparticles often interact with cells through the following process: first, nanoparticles adhere to the cell membrane and trigger cell reactions such as endocytosis. The adhesion and endocytosis of nanocrystals are significantly affected by ambient temperature.[21] Endocytosis of cells is inhibited at 4 °C, and only nonspecific binding is preserved;[22] at 37 °C, the nonspecific binding between the cell membrane and nanoparticles is inhibited, while active endocytosis is not restricted, and it can show a linear growth trend.[21,23]

COM crystals were labeled with FITC and showed green fluorescence (Figure 9). The cells were incubated at 4 °C, and the distribution of COM crystals on the cell membrane was observed by CLSM (Figure 10). The observed crystals were all adhered crystals, because endocytosis was inhibited at 4 °C. A large number of COM crystals were adhered to the injured cells, and the crystals were aggregated, but the adhesion crystals of the cells in the polysaccharide protection group were obviously reduced. The higher the polysaccharide concentration, the lesser is the crystal adhesion. At the same concentration, the adhesion inhibition effect of CCSP3 was better than that of CSP0.

3.10. Quantitative Detection of Cell Proportion of Adhered Crystals. FITC was used to fluorescently label nano-COM crystals (Figure 9), and the percentage of cells with adhered nano-COM crystals was quantitatively detected by flow cytometry (Figure 11). The percentage of cells with adhered nano-COM crystals in the injured group with added COM crystals was the highest (57.4%). By contrast, the percentage of cells was only 0.31% with adhered nano-COM crystals in the normal group. After CSP0 or CCSP3 treatment, the proportion of cells with adhered nano-COM crystals decreased significantly (from 21.6 to 50.4%) ($p < 0.01$), that is, polysaccharides inhibited the crystal adhesion (Figure 11B). At the same concentration, CCSP3 can inhibit the adhesion of HK-2 cells to crystals more strongly than CSP0.

https://doi.org/10.1021/acsomega.4c00110
ACS Omega 2024, 9, 19236−19249

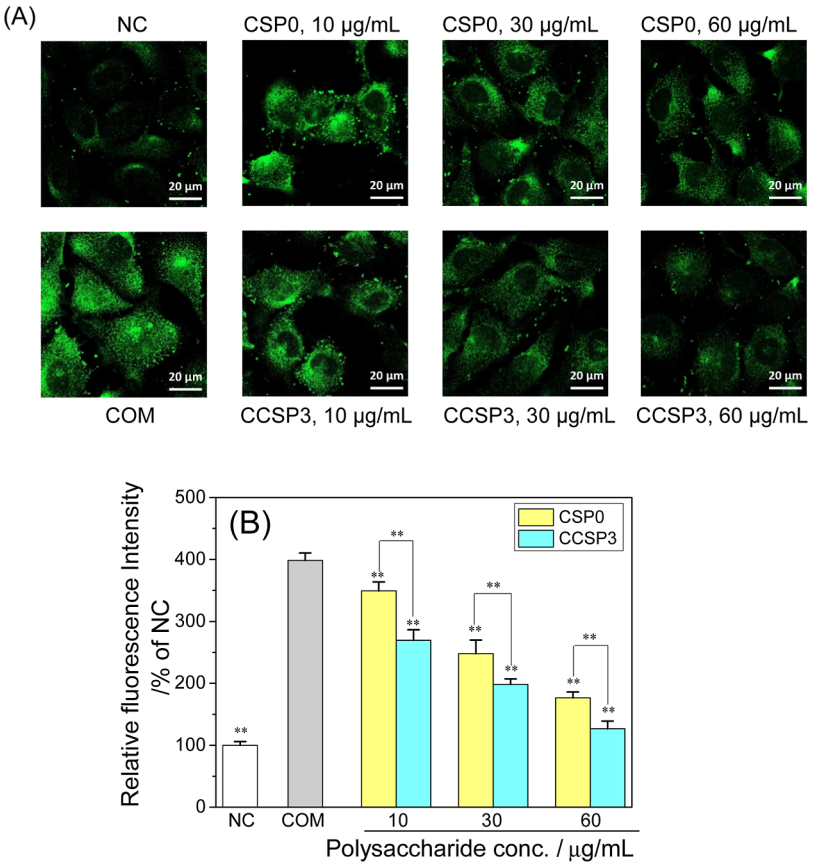

Figure 7. Changes in the OPN expression of HK-2 cells before and after CSP0 and CCSP3 protection were detected. (A) The OPN expression was observed by CLSM. (Scale bars: 20 μm). (B) Quantitative histogram of OPN relative fluorescence intensity. NC. Nano-COM concentration: 200 μg/mL. Protection time: 12 h. Compared with the COM group, $^{**}p < 0.01$.

At different concentrations, there was a concentration-dependent effect on the ability of polysaccharides to inhibit crystal adhesion on HK-2 cells. That is, the best inhibition effect was found at the largest concentration of 60 μg/mL. For example, after 60 μg/mL CSP0 or CCSP3 protection, the proportion of cells adhering to the crystals was 30.2 and 21.6%, respectively.

3.11. Observation of the Crystal Adhesion by SEM. SEM was used to observe the crystal adhesion of HK-2 cells protected by different concentrations of CSP0 and CCSP3 (Figure 12). After treatment with nano-COM crystals for 12 h, a large number of crystals adhered to the surface of unprotected cells and the adhered crystals were seriously clustered. Under the combined action of polysaccharides and crystals, the number of crystals that adhered to the cell surface decreased and the crystals were dispersed. Compared with CSP0, under the protection of CCSP3, the cells adhered to fewer crystals and more tightly, and the adhered crystals gradually decreased with the increase in polysaccharide concentration.

Thus, carboxymethylated CSPs not only inhibit the adhesion of HK-2 cells to COM crystals but also inhibit the aggregation of crystals on the cell surface.

4. DISCUSSION

4.1. CCSPs Inhibit Oxidative Stress Induced by COM Crystals. Studies have shown that some natural polysaccharides have better or wider biological activities after molecular modification through carboxymethylation, sulfonation, or phosphorylation.[24] In the current study, CSPs modified by carboxymethylation showed higher activities than nonmodified ones in protecting cells from the damage caused by nano-COM crystals. This ability is attributed to the high −COOH content in polysaccharides that provides additional reducing functional groups that can accept and eliminate free radicals.[25]

Because micron crystals have a smaller damage effect on cells than nanocrystals,[26,27] and crystals with more negative charges on the crystal surface (i.e., more negative zeta potential) have a smaller damage effect on cells,[28,29] therefore, a higher concentration of CCSP3 (such as 60 μg/mL) was more effective in protecting HK-2 cells from nano-COM-free damage.

ROS are potentially dangerous in the formation of renal tubular epithelial cells and kidney calculi induced by crystals.[30] For example, CaOx crystals can induce autophagy by activating the ROS pathway in cells and aggravate the damage of renal epithelial cells.[31] COM crystals resulted in an increase in the ROS level (Figure 2) and a decrease in the mitochondrial membrane potential (Figure 6). CSP0 and CCSP3 can effectively inhibit these changes.

Mitochondria are the main source of ROS production in cells.[32] Excessive production of ROS results in oxidative stress, which may lead to an inflammatory reaction.[33] Moreover, the mitochondrial stress pathway of cells may be activated by ROS and other free radicals, which may further cause mitochondrial damage.[34] Guo et al.[35] also showed that corn stigma polysaccharide can inhibit the decrease in mitochondrial membrane potential induced by H_2O_2 and inhibit oxidative stress by increasing the enzyme activities of SOD, CAT, and GPX. Our results confirm that CSP0 and CCSP3 can reduce

https://doi.org/10.1021/acsomega.4c00110
ACS Omega 2024, 9, 19236−19249

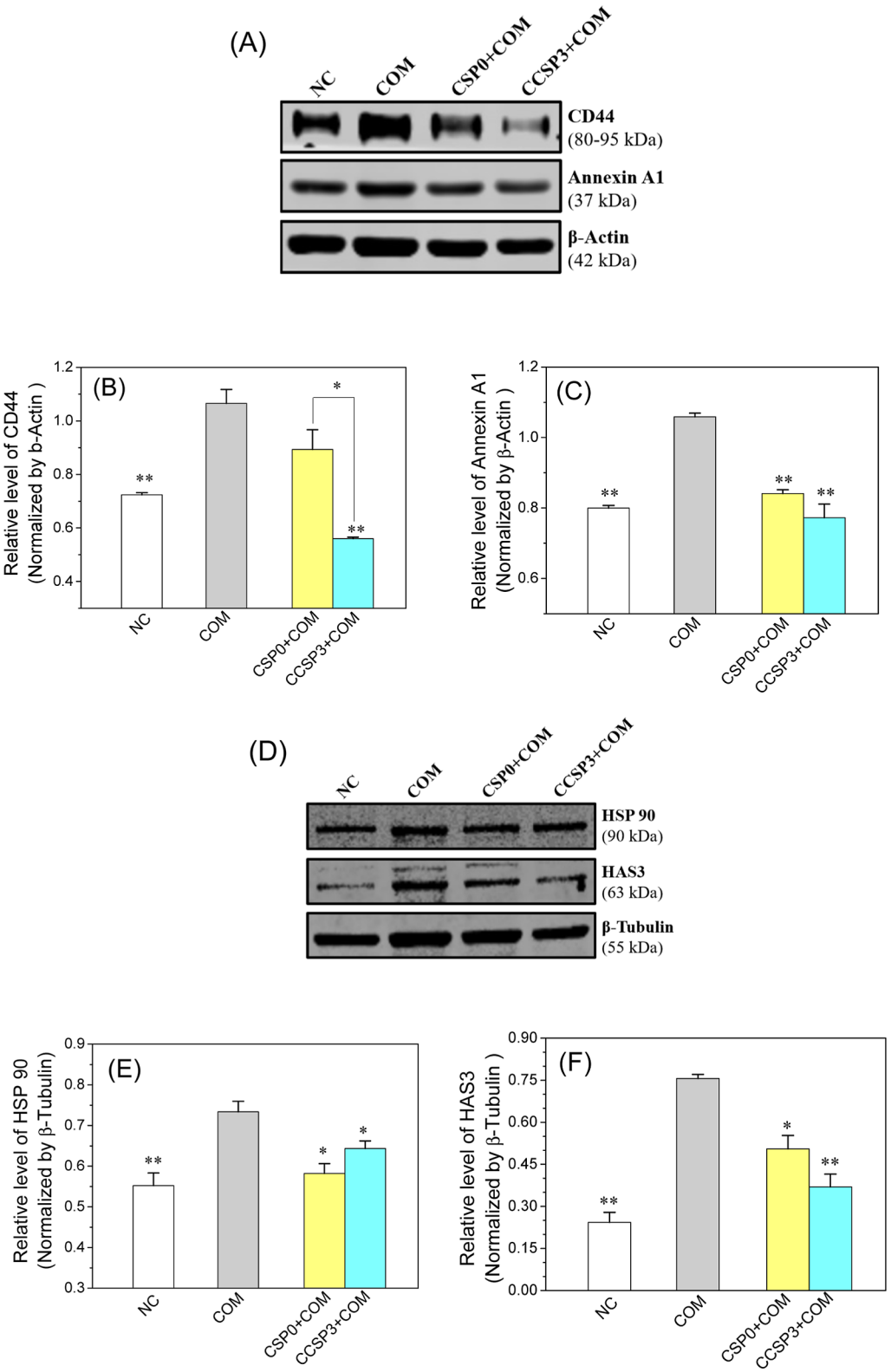

Figure 8. Western blot analysis was used to detect the expression of crystal adhesion-related proteins (Annexin A1, HSP90, HAS3, and CD44) in HK-2 cells before and after CSP0 and CCSP3 protection. (A) Western blot bands of CD44, Annexin A1, and β-Actin. (B) Histogram of relative expression of CD44. (C) Histogram of relative expression of Annexin A1. (D) Western blot bands of HSP90, HAS3, and β-Tubulin. (E) Histogram of relative expression of HSP90. (F) Histogram of relative expression of HAS3. NC. Nano-COM concentration: 200 μg/mL. Protection time: 12 h. Compared with the COM group, $^{*}p < 0.05$; $^{**}p < 0.01$.

mitochondrial damage, thus inhibiting the oxidative stress induced by COM crystals.

4.2. CCSPs Can Reduce Cell Damage Induced by COM Crystals and Promote Cell Proliferation. The activity of HK-2 cells was reduced by nano-COM crystals (Figure 1),

https://doi.org/10.1021/acsomega.4c00110
ACS Omega 2024, 9, 19236−19249

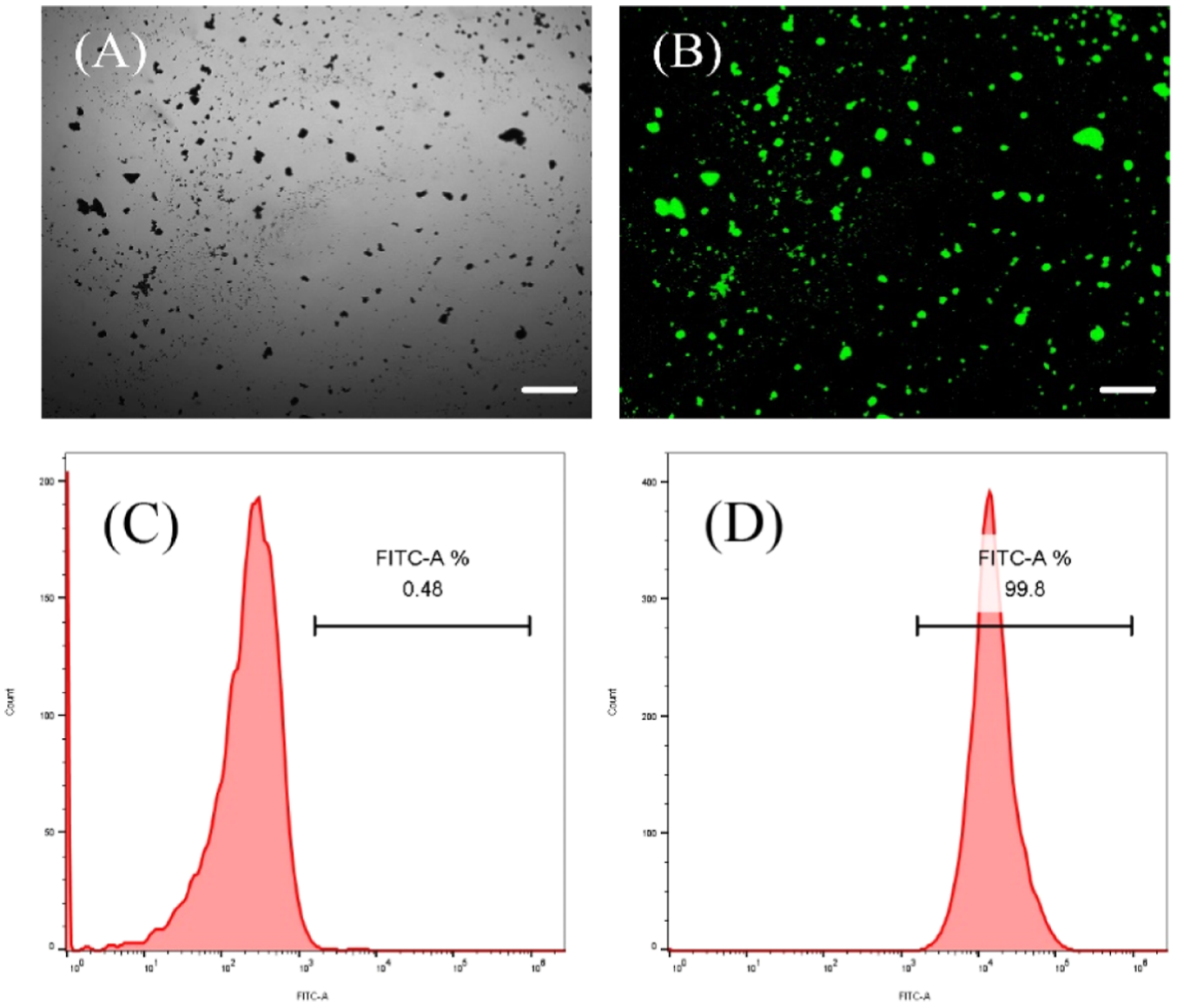

Figure 9. Nano-COM crystals were labeled with FITC. Microscopic photos (A,B) and flow cytometry histograms (C,D) of nano-COM crystals before and after labeling (scale bars: 20 μm).

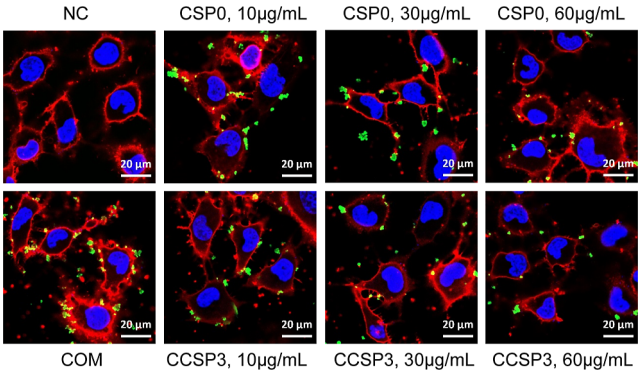

Figure 10. Distribution of nano-COM crystals on the cell membrane before and after CSP0 and CCSP3 protection was observed by CLSM. (Scale bars: 20 μm). NC. Nano-COM concentration: 200 μg/mL. Protection time: 12 h.

which resulted in deformation of the cytoskeleton, disorder of actin distribution (Figure 3), and increased eversion of PS (Figure 4).

Actin is a ubiquitous cytoskeleton protein in various cells, which plays an important role in the establishment and maintenance of normal physiological functions of cells.[36] The destruction of the cytoskeleton may cause various cell injuries. Ordonez et al.[37] showed that the abnormality of actin may induce mitochondrial dysfunction and neuronal death and eventually lead to Parkinson's disease. PS is one of the phospholipids distributed asymmetrically on the cell membrane. PS is almost only located in the inner leaf of the plasma membrane.[38] However, in apoptotic cells, PS will turn from the inner leaf to the outer leaf of the plasma membrane and be exposed to the external environment of cells. Studies have shown that PS eversion plays an important role in CaOx urolithiasis caused by hyperoxaluria.[39] Our results showed that under the protection of polysaccharides, the cell morphology gradually became full, the actin gradually became clear (Figure 3), and PS

https://doi.org/10.1021/acsomega.4c00110
ACS Omega 2024, 9, 19236−19249

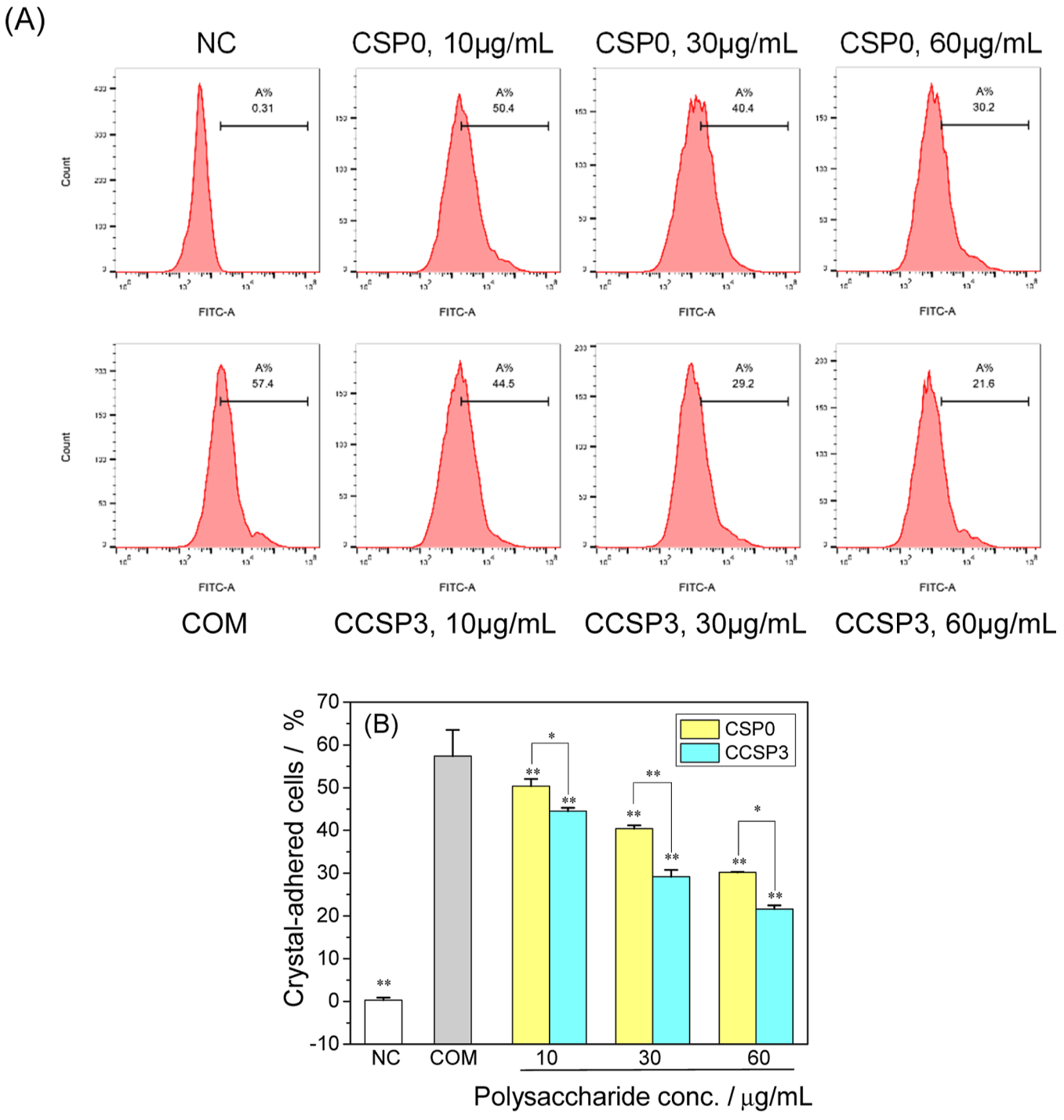

Figure 11. Quantitative detection of the percentage of cells with adhered nano-COM crystals before and after CSP0 and CCSP3 protection. (A) Flow cytometry histogram. (B) Quantitative histogram of crystal adhesion. NC. Nano-COM concentration: 200 μg/mL. Protection time: 12 h. Compared with the COM group, $^{*}p < 0.05$; $^{**}p < 0.01$.

eversion was inhibited (Figure 4), which indicated that CSP0 and CCSP3 reduced the cell damage induced by COM crystals.

Cell proliferation is recognized as an important healing process in several important diseases, such as acute kidney injury.[6] The cell cycle is the main process of cell proliferation, which is an orderly series of events occurring in different stages that finally leads to a cell dividing into two daughter cells.[40] Our analysis of the cell cycle of HK-2 showed that the damage of nano-COM crystals caused more cells to stay in the *S* phase and decreased the number of *G*1-phase cells, which promoted the cell cycle transition of HK-2 cells from *G*2/*M* and *S* phase to *G*1 phase after CSP0 or CCSP3 protection (Figure 5). The *S* phase is a process of DNA synthesis, and a large number of cells in the *S* phase indicate that DNA synthesis is interrupted, which will halt cell proliferation. The *G*2/*M* stage is the late stage of DNA synthesis and mitotic stage. Stagnation of the tubular cell cycle in the *G*2/*M* phase may lead to the production of fibrosis factors, such as connective tissue growth factor and transforming growth factor (TGF-β), which will lead to acute kidney injury or renal fibrosis.[41] However, the proportion of G2/M cells decreased

https://doi.org/10.1021/acsomega.4c00110
ACS Omega 2024, 9, 19236−19249

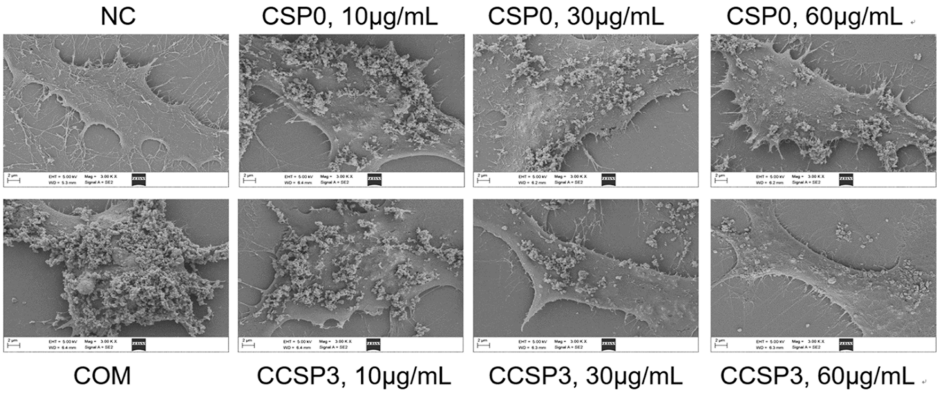

Figure 12. SEM observation of the inhibition of adhesion and aggregation of nano-COM crystals after different concentrations of CSP0 and CCSP3 protection. Scale bars: 2 μm. Nano-COM concentration: 200 μg/mL. Protection time: 12 h.

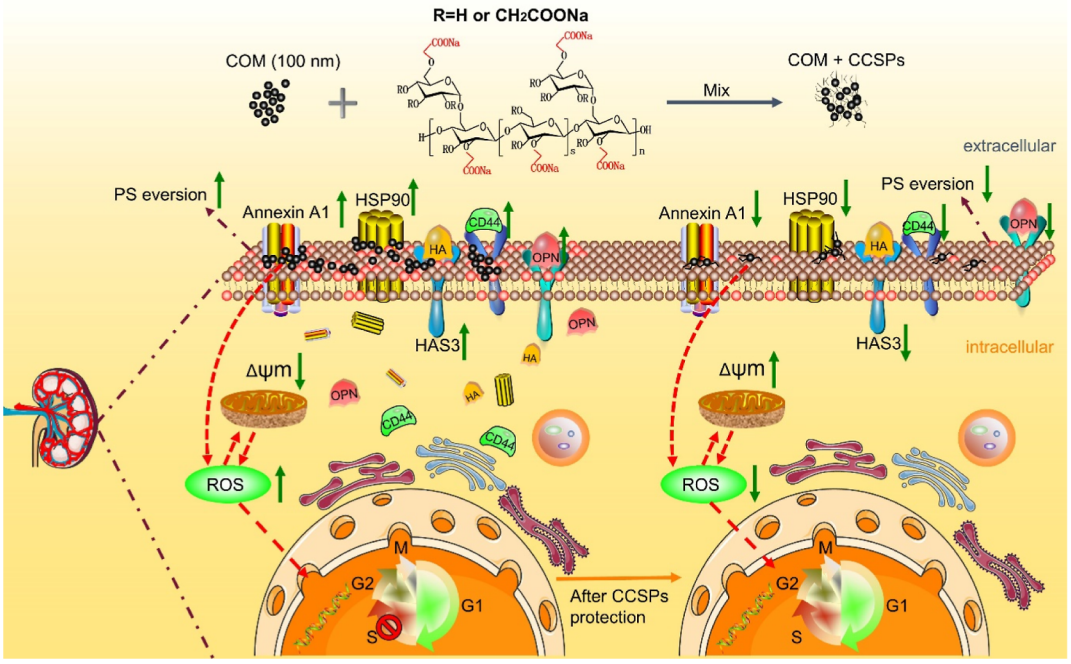

Figure 13. Schematic diagram of the mechanism of inhibiting the adhesion and aggregation of nano-COM crystals on the HK-2 cell surface before and after CCSP protection.

from 15.8 to 7.72% after CCSP3 protection (Figure 5), which means that CCSP3 helps to prevent HK-2 cells from blocking in the *G2/M* phase. Therefore, we believe that CCSPs can accelerate the DNA synthesis process of HK-2 cells, promote cell proliferation, and reduce the risk of acute kidney injury or renal fibrosis.

4.3. CCSPs Reduce Crystal Adhesion by Inhibiting the Expression of Adhesion-Related Proteins. The adhesion of COM crystals on the surface of renal epithelial cells is one of the key steps in the formation of kidney calculi.[25,42] The adhesion enhancement of CaOx crystals to the renal tubular epithelial cells is realized by the overexpression of adhesion molecules induced by the crystals, among which OPN, CD44, and HA are representative adhesion molecules.[5,43] In addition, Annexin A1 and HSP90 expression on the surface of renal tubular epithelial cells can act as potential receptors of CaOx crystals and participates in the activation of NF-κB and mitotic activated protein kinase (MAPK), which leads to cell reactions, such as cell damage and cell cycle retention, after crystal adhesion.[44,45] Our results indicated that the interaction of COM crystals with HK-2 cells upregulated the expression levels of OPN (Figure 7), CD44, HAS3, Annexin A1, and HSP90 (Figure 8). As one of the main synthetic sources of HA, HAS3 is involved in cell adhesion and signal transduction.[46] The increased expression of the five adhesion-related proteins leads to increased adhesion of COM crystals on the cell membrane (Figures 10−12), thereby increasing the risk of stone formation. El-Salam et al.[47] showed that 3,4,5-triphthalic acid methyl ester reduced the adhesion of cells to CaOx crystals by downregulating Annexin A1 expression on the surface of kidney cells. Similarly, Mulay et al.[48] showed that blocking TNF receptor signal inhibited the expression and mRNA transcription of CD44 and Annexin II in renal tubular epithelial cells in vitro and in vivo, thus protecting hyperoxaluria mice from chronic kidney disease. Our study shows that CSP0 or CCSP3 can inhibit the expression of these adhesion-related proteins, thereby reducing the adhesion of crystals to cells and the risk of kidney calculi formation.

Carboxymethylated CCSP3 inhibited the expression of four proteins, aside from HSP90, compared to the unmodified CSP0. Peerapen and Thongboonkerd[45] obtained similar results by

https://doi.org/10.1021/acsomega.4c00110
ACS Omega 2024, 9, 19236−19249

protein blotting and immunofluorescence. Caffeine specifically affects Annexin A1 expression on the cell membrane but does not affect the expression of other COM crystal-binding proteins (Annexin A2, α-enolase, HSP70, and HSP90). Although the mechanism through which the −COOH content in polysaccharides affects the expression of adhesion-related proteins remains unclear, the protective effect of CCSP3 is actually better than that of CSP0.

According to the results of this study, we proposed the mechanism of CCSP inhibition of kidney epithelial cell injury and crystal adhesion induced by nano-COM crystals (Figure 13). CCSPs can reduce ROS production in cells, maintain the mitochondrial membrane potential and actin cytoskeleton, and promote cell proliferation, thus improving cell vitality. Under the protection of CSP0 and CCSP3, the eversion of PS and the expression of adhesion-related proteins (OPN, CD44, HAS3, Annexin A1, and HSP90) were reduced, thus inhibiting cell adhesion to the COM crystal. The results show that CCSPs can reduce the risk of CaOx stone formation by protecting kidney cells from CaOx crystal damage and inhibiting crystal adhesion.

5. CONCLUSIONS

CSP0 and CCSP3 can effectively reduce the damage of HK-2 cells caused by nano-COM crystals, and the CCSP3 with a high content of −COOH (16.38%) or high concentration of polysaccharides had a better effect. Under the protection of CSP0 or CCSP3, the decrease in cell vitality, cytoskeleton destruction, increase in the ROS level, PS eversion, and cell cycle retention caused by COM crystals were inhibited and the number of COM crystals that adhered to the cell surface was reduced. CSP0 or CCSP3 can reduce crystal adhesion by inhibiting the expression of adhesion-related proteins (OPN, CD44, Annexin A1, HSP90, and HAS3) caused by COM crystals. CCSPs can inhibit stone formation by inhibiting the damage and adhesion of COM crystals to renal cells. Thus, CCSPs have potential application value in inhibiting the formation and recurrence of CaOx stones.

AUTHOR INFORMATION

Corresponding Authors

Fan-Yu Wu − *Yingde Center, Institute of Kidney Surgery, Jinan University, Guangdong 510000, China; Department of Urology, People's Hospital of Yingde City, Yingde 513000, China*; Email: ydwolf@126.com

Jian-Ming Ouyang − *Institute of Biomineralization and Lithiasis Research, Jinan University, Guangzhou 510632, China*; orcid.org/0000-0001-8075-3915; Email: toyjm@jnu.edu.cn

Authors

Bao-Li Heng − *Yingde Center, Institute of Kidney Surgery, Jinan University, Guangdong 510000, China; Department of Urology, People's Hospital of Yingde City, Yingde 513000, China*

Xin-Yi Tong − *Institute of Biomineralization and Lithiasis Research, Jinan University, Guangzhou 510632, China*

Guo-Jun Zou − *Institute of Biomineralization and Lithiasis Research, Jinan University, Guangzhou 510632, China*

Complete contact information is available at: https://pubs.acs.org/10.1021/acsomega.4c00110

Notes

The authors declare no competing financial interest.

ACKNOWLEDGMENTS

This work was supported by the National Natural Science Foundation of China (nos. 82270800 and 21975105) and the Science and Technology Project of Qingyuan City, Guangdong Province, China (no: 2022KJJH033) and the Medical Scientific Research Foundation of Guangdong Province, China (no: B2021102).

REFERENCES

(1) Siener, R. Nutrition and kidney stone disease. *Nutrients* **2021**, *13* (6), 1917.

(2) Schubert, G. Stone analysis. *Urol. Res.* **2006**, *34* (2), 146−150.

(3) Sun, X. Y.; Gan, Q. Z.; Ouyang, J. M. Calcium oxalate toxicity in renal epithelial cells: the mediation of crystal size on cell death mode. *Cell Death Discovery* **2015**, *1*, 15055.

(4) Qi, S.; Wang, Q.; Xie, B.; Chen, Y.; Zhang, Z.; Xu, Y. P38 MAPK signaling pathway mediates COM crystal-induced crystal adhesion change in rat renal tubular epithelial cells. *Urolithiasis* **2020**, *48* (1), 9−18.

(5) Wang, Z.; Zhang, J.; Zhang, Y.; Deng, Q.; Liang, H. Expression and mutations of BRCA in breast cancer and ovarian cancer: Evidence from bioinformatics analyses. *Int. J. Mol. Med.* **2018**, *48* (2), 1−10.

(6) Khamchun, S.; Thongboonkerd, V. Cell cycle shift from G0/G1 to S and *G2/M* phases is responsible for increased adhesion of calcium oxalate crystals on repairing renal tubular cells at injured site. *Cell Death Discovery* **2018**, *4*, 106.

(7) Sheng, X.; Jung, T.; Wesson, J. A.; Ward, M. D. Adhesion at calcium oxalate crystal surfaces and the effect of urinary constituents. *Proc. Natl. Acad. Sci. U.S.A.* **2005**, *102* (2), 267−272.

(8) Liu, Y.; Ding, C.; He, L.; Yang, X.; Gou, Y.; Xu, X.; Liu, Y.; Zhao, C.; Li, J.; Li, J. Bioinspired heptapeptides as functionalized mineralization inducers with enhanced hydroxyapatite affinity. *J. Mater. Chem. B* **2018**, *6* (13), 1984−1994.

(9) Duan, Z. H.; Duan, W. W.; Li, F. P.; Li, Y. Q.; Luo, P.; Liu, H. Z. Effect of carboxymethylation on properties of fucoidan from Laminaria japonica: Antioxidant activity and preservative effect on strawberry during cold storage. *Postharvest Biol. Technol.* **2019**, *151*, 127−133.

(10) Theis, T. V.; Santos, V. A. Q.; Appelt, P.; Barbosa-Dekker, A.; Vetvicka, V.; Dekker, R.; Cunha, M. A. Fungal Exocellular (1-6)-*β*-d-glucan: Carboxymethylation, Characterization, and Antioxidant Activity. *Int. J. Mol. Sci.* **2019**, *20* (9), 2337.

(11) Sun, X.; Zhao, C.; Pan, W.; Wang, J.; Wang, W. Carboxylate groups play a major role in antitumor activity of Ganoderma applanatum polysaccharide. *Carbohydr. Polym.* **2015**, *123*, 283−287.

(12) Zhang, D.; Wang, Y.; Liu, H. Corn silk extract inhibit the formation of Nε-carboxymethyllysine by scavenging glyoxal/methyl glyoxal in a casein glucose-fatty acid model system. *Food Chem.* **2020**, *309*, 125708.

(13) Saheed, S.; Oladipipo, A. E.; Abdulazeez, A. A.; Olarewaju, S. A.; Ismaila, N. O.; Emmanuel, I. A.; Fatimah, Q. D.; Aisha, A. Y. Toxicological evaluations of Stigma maydis (corn silk) aqueous extract on hematological and lipid parameters in Wistar rats. *Toxicol Rep* **2015**, *2*, 638−644.

(14) Pan, Y.; Wang, C.; Chen, Z.; Li, W.; Yuan, G.; Chen, H. Physicochemical properties and antidiabetic effects of a polysaccharide from corn silk in high-fat diet and streptozotocin-induced diabetic mice. *Carbohydr. Polym.* **2017**, *164*, 370−378.

(15) Chen, J.-Y.; Sun, X.-Y.; Ouyang, J.-M. Modulation of calcium oxalate crystal growth and protection from oxidatively damaged renal epithelial cells of corn silk polysaccharides with different molecular weights. *Oxid. Med. Cell. Longev.* **2020**, *2020*, 1−19.

(16) Li, J.; Shang, W. T.; Si, X.; Bu, D. D.; Strappe, P.; Zhou, Z. K.; Blanchard, C. Carboxymethylation of corn bran polysaccharide and its bioactive property. *Int. J. Food Sci. Technol.* **2017**, *52* (5), 1176−1184.

(17) Zou, G.-J.; Huang, W.-B.; Sun, X.-Y.; Tang, G.-H.; Ouyang, J.-M. Carboxymethylation of corn silk polysaccharide and its inhibition on adhesion of nanocalcium oxalate crystals to damaged renal epithelial cells. *ACS Biomater. Sci. Eng.* **2021**, *7*, 3409−3422.

(18) Sun, X.-Y.; Ouyang, J.-M.; Liu, A.-J.; Ding, Y.-M.; Gan, Q. Z.; Gan, Q.-Z. Preparation, characterization, and in vitro cytotoxicity of COM and COD crystals with various sizes. *Mater. Sci. Eng., C* **2015**, *57*, 147−156.
(19) Vinaiphat, A.; Thongboonkerd, V. Characterizations of PMCA2-interacting complex and its role as a calcium oxalate crystal-binding protein. *Cell. Mol. Life Sci.* **2018**, *75* (8), 1461−1482.
(20) Zhang, H.; Sun, X. Y.; Chen, X. W.; Ouyang, J. M. Degraded Porphyra yezoensis polysaccharide protects HK-2 cells and reduces nano-COM crystal toxicity, adhesion and endocytosis. *J. Mater. Chem. B* **2020**, *8* (32), 7233−7252.
(21) Sommi, P.; Vitali, A.; Coniglio, S.; Callegari, D.; Barbieri, S.; Casu, A.; Falqui, A.; Vigano', L.; Vigani, B.; Ferrari, F.; Anselmi-Tamburini, U. Microvilli adhesion: an alternative route for nanoparticle cell internalization. *ACS Nano* **2021**, *15* (10), 15803−15814.
(22) Lesniak, A.; Salvati, A.; Santos-Martinez, M. J.; Radomski, M. W.; Dawson, K. A.; Åberg, C. Nanoparticle adhesion to the cell membrane and its effect on nanoparticle uptake efficiency. *J. Am. Chem. Soc.* **2013**, *135* (4), 1438−1444.
(23) Salvati, A.; Aberg, C.; dos Santos, T.; Varela, J.; Pinto, P.; Lynch, I.; Dawson, K. A. Experimental and theoretical comparison of intracellular import of polymeric nanoparticles and small molecules: toward models of uptake kinetics. *Nanomedicine* **2011**, *7* (6), 818−826.
(24) Cheng, H.; Huang, G. The antioxidant activities of carboxymethylated garlic polysaccharide and its derivatives. *Int. J. Biol. Macromol.* **2019**, *140*, 1054−1063.
(25) Sun, X. Y.; Zhang, H.; Liu, J.; Ouyang, J. M. Repair activity and crystal adhesion inhibition of polysaccharides with different molecular weights from red algae Porphyra yezoensis against oxalate-induced oxidative damage in renal epithelial cells. *Food Funct.* **2019**, *10* (7), 3851−3867.
(26) Sun, X. Y.; Chen, J. Y.; Rao, C. Y.; Ouyang, J. M. Size-Dependent Cytotoxicity of Hydroxyapatite Crystals on Renal Epithelial Cells. *Int. J. Nanomed.* **2020**, *15*, 5043−5060.
(27) Sun, X. Y.; Gan, Q. Z.; Ouyang, J. M. Calcium oxalate toxicity in renal epithelial cells: the mediation of crystal size on cell death mode. *Cell Death Discovery* **2015**, *1*, 15055.
(28) Sun, X. Y.; Ouyang, J. M.; Liu, A. J.; Ding, Y. M.; Gan, Q. Z. Preparation, characterization, and in vitro cytotoxicity of COM and COD crystals with various sizes. *Mater. Sci. Eng., C* **2015**, *57*, 147−156.
(29) Damaceanu, M.; Mihai, M.; Popescu, I.; Brumă, M.; Schwarz, S. Synthesis and characterization of a new oxadiazole-functionalized maleic anhydride-N-vinylpyrrolidone copolymer and its application in $CaCO_3$ based microparticles. *React. Funct. Polym.* **2012**, *72*, 635−641.
(30) Wu, J.; Tao, Z.; Deng, Y.; Liu, Q.; Liu, Y.; Guan, X.; Wang, X. Calcifying nanoparticles induce cytotoxicity mediated by ROS-JNK signaling pathways. *Urolithiasis* **2019**, *47* (2), 125−135.
(31) Liu, Y.; Li, D.; He, Z.; Liu, Q.; Wu, J.; Guan, X.; Tao, Z.; Deng, Y. Inhibition of autophagy-attenuated calcium oxalate crystal-induced renal tubular epithelial cell injury in vivo and in vitro. *Oncotarget* **2018**, *9* (4), 4571−4582.
(32) Vakifahmetoglu-Norberg, H.; Ouchida, A. T.; Norberg, E. The role of mitochondria in metabolism and cell death. *Biochem. Biophys. Res. Commun.* **2017**, *482* (3), 426−431.
(33) Albert, A.; Paul, E.; Rajakumar, S.; Saso, L. Oxidative stress and endoplasmic stress in calcium oxalate stone disease: the chicken or the egg? *Free Radic. Res.* **2020**, *54* (4), 244−253.
(34) Hernansanz-Agustín, P.; Enríquez, J. A. Generation of reactive oxygen species by mitochondria. *Antioxidants* **2021**, *10* (3), 415.
(35) Guo, Q.; Xu, L.; Chen, Y.; Ma, Q.; Santhanam, R. K.; Xue, Z.; Gao, X.; Chen, H. Structural characterization of corn silk polysaccharides and its effect in H_2O_2 induced oxidative damage in L6 skeletal muscle cells. *Carbohydr. Polym.* **2019**, *208*, 161−167.
(36) Peerapen, P.; Thongboonkerd, V. Calcium oxalate monohydrate crystal disrupts tight junction via F-actin reorganization. *Chem. Biol. Interact.* **2021**, *345*, 109557.
(37) Ordonez, D. G.; Lee, M. K.; Feany, M. B. α-synuclein Induces Mitochondrial Dysfunction through Spectrin and the Actin Cytoskeleton. *Neuron* **2018**, *97* (1), 108−124.
(38) Chen, Y. Z.; Kloditz, K.; Lee, E. S.; Nguyen, D. P.; Yuan, Q.; Johnson, J.; Lee-Yow, Y.; Hall, A.; Mitani, S.; Xia, N. S.; Fadeel, B.; Xue, D. Structure and function analysis of the C. elegans aminophospholipid translocase TAT-1. *J. Cell Sci.* **2019**, *132* (5), jcs227660.
(39) Li, Y.; Yu, S.; Gan, X.; Zhang, Z.; Wang, Y.; Wang, Y.; An, R. MRP-1 and BCRP promote the externalization of phosphatidylserine in oxalate-treated renal epithelial cells: implications for calcium oxalate urolithiasis. *Urology* **2017**, *107*, 271.e9−271.e17.
(40) Hustedt, N.; Durocher, D. The control of DNA repair by the cell cycle. *Nat. Cell Biol.* **2017**, *19* (1), 1−9.
(41) Canaud, G.; Bonventre, J. V. Cell cycle arrest and the evolution of chronic kidney disease from acute kidney injury. *Nephrol. Dial. Transplant.* **2015**, *30* (4), 575−583.
(42) Zhang, H.; Sun, X. Y.; Ouyang, J. M. Effects of porphyra yezoensis polysaccharide with different molecular weights on the adhesion and endocytosis of nanocalcium oxalate monohydrate in repairing damaged HK-2 cells. *ACS Biomater. Sci. Eng.* **2019**, *5* (8), 3974−3986.
(43) Tsuji, H.; Shimizu, N.; Nozawa, M.; Umekawa, T.; Yoshimura, K.; De Velasco, M. A.; Uemura, H.; Khan, S. R. Osteopontin knockdown in the kidneys of hyperoxaluric rats leads to reduction in renal calcium oxalate crystal deposition. *Urolithiasis* **2014**, *42* (3), 195−202.
(44) Fong-Ngern, K.; Sueksakit, K.; Thongboonkerd, V. Surface heat shock protein 90 serves as a potential receptor for calcium oxalate crystal on apical membrane of renal tubular epithelial cells. *J. Biol. Inorg. Chem.* **2016**, *21* (4), 463−474.
(45) Peerapen, P.; Thongboonkerd, V. Caffeine prevents kidney stone formation by translocation of apical surface annexin A1 crystal-binding protein into cytoplasm: In vitro evidence. *Sci. Rep.* **2016**, *6*, 38536.
(46) Wang, Y.; Wang, F.; Xu, S.; Wang, R.; Tian, C.; Ji, Y.; Yang, Q.; Zhao, P.; Xia, Q. Transdermal peptide conjugated to human connective tissue growth factor with enhanced cell proliferation and hyaluronic acid synthesis activities produced by a silkworm silk gland bioreactor. *Appl. Microbiol. Biotechnol.* **2020**, *104* (23), 9979−9990.
(47) El-Salam, M. A.; Bastos, J. K.; Han, J. J.; Previdi, D.; Coelho, E. B.; Donate, P. M.; Romero, M. F.; Lieske, J. The synthesized plant metabolite 3,4,5-tri-o-galloylquinic acid methyl ester inhibits calcium oxalate crystal growth in a drosophila model, downregulates renal cell surface Annexin A1 expression, and decreases crystal adhesion to cells. *J. Med. Chem.* **2018**, *61* (4), 1609−1621.
(48) Mulay, S. R.; Eberhard, J. N.; Desai, J.; Marschner, J. A.; Kumar, S. V.; Weidenbusch, M.; Grigorescu, M.; Lech, M.; Eltrich, N.; Muller, L.; Hans, W.; de Angelis, M. H.; Vielhauer, V.; Hoppe, B.; Asplin, J.; Burzlaff, N.; Herrmann, M.; Evan, A.; Anders, H. J. Hyperoxaluria requires TNF receptors to initiate crystal adhesion and kidney stone disease. *J. Am. Soc. Nephrol.* **2017**, *28* (3), 761−768.

https://doi.org/10.1021/acsomega.4c00110
ACS Omega 2024, 9, 19236−19249